ISSN 1070-3284, Russian Journal of Coordination Chemistry, 2018, Vol. 44, No. 4, pp. 301–315. © Pleiades Publishing, Ltd., 2018.
Original Russian Text © S.A. Lermontova, I.S. Grigor'ev, E.Yu. Ladilina, I.V. Balalaeva, N.Yu. Shilyagina, L.G. Klapshina, 2018, published in Koordinatsionnaya Khimiya, 2018, Vol. 44, No. 2, pp. 151–166.

Porphyrazine Structures with Electron-Withdrawing Substituents as the Base for Materials for Photonics and Biomedicine

S. A. Lermontova[a, b], I. S. Grigor'ev[b], E. Yu. Ladilina[b], I. V. Balalaeva[a], N. Yu. Shilyagina[a], and L. G. Klapshina[a, b, *]

[a] *Lobachevsky State University of Nizhny Novgorod, Nizhny Novgorod, 603950 Russia*
[b] *Razuvaev Institute of Organometallic Chemistry, Russian Academy of Sciences, Nizhny Novgorod, 603950 Russia*
**e-mail: klarisa@iomc.ras.ru*

Received October 3, 2017

Abstract—A survey of the studies dealing with the development of new porphyrazine type tetrapyrrole dyes promising for the application in photonics and biophotonics is presented. An original synthetic approach to the template assembly of the porphyrazine macrocycle at room temperature in high yield has been proposed. A porphyrazine macrocycle containing eight nitrile groups at the periphery has been prepared for the first time. The replacement of four nitrile groups in the macrocycle by aryl groups has been found to generate a unique porphyrazine structure demonstrating a fluorescent molecular rotor behavior, i.e., a strong dependence of fluorescence parameters (quantum yields and lifetimes) on the viscosity of the medium. Some aspects of possible applications of the obtained compounds in biophotonics are described. Good prospects for the use of these compounds as efficient agents for tumor diagnosis, sensitizers for photodynamic therapy, and probes for intracellular viscosity are outlined.

Keywords: porphyrazines, template synthesis, ytterbium complexes, optical teranostic agents, photosensitizers, optical probes for intracellular viscosity

DOI: 10.1134/S1070328418040061

INTRODUCTION

The extensive class of tetrapyrrole macrocycles occupies a central position in the modern organic and bioorganic chemistry. This is related to the wide use of these compounds as light-absorbing, non-linear optical, and luminescent materials in laser physics and optoelectronics [1, 2]. Numerous medical applications of tetrapyrroles utilizing their interaction with light are also well known [3].

This review is devoted to the studies carried out in the last 10 years at the Razuvaev Institute of Organometallic Chemistry, Russian Academy of Sciences (IOMC RAS), on the development of new porphyrazine type tetrapyrrole compounds possessing unique electrochemical and photophysical properties and application of these compounds in photonic and biophotonic technologies. An original synthetic approach has been proposed for the template assembly of new cyanoporphyrazine macrocycles at room temperature with high yields of the target products [4]. Octacyanoporphyrazine macrocycles were obtained and characterized for the first time as vanadyl and ytterbium(III) complexes. In this case, tetracyanoethylene molecules were used as macrocycle structural units in the template assembly. The obtained compounds exhibit strong electron-withdrawing properties, which is unusual for this class of macroheterocycles [5]. The use of diversified aryltricyanoethylenes as structural units gave rise to a broad series of luminescent tetraaryltetracyanoporphyrazines as free bases and metal complexes, which are high-performance singlet oxygen ptotosensitizers, with the sensitivity of fluorescence parameters to the environment viscosity being unique for tetrapyrrole macrocycles. Therefore, in the last several years, the research team comprising synthetic chemists, biophysicists, laser spectroscopists, and biomedical scientists has been actively promoting the compounds developed at the IOMC RAS as potential agents for personalized cancer therapy.

CYANOPORPHYRAZINE VANADYL COMPLEXES

Among tetrapyrrole macrocycles, porphyrazines have long remained the least studied compounds in comparison with porphyrins and phthalocyanines, which are widely presented in the literature. In the last two decades, a considerable contribution to the investigation of this class of tetrapyrroles was made by A. Barrett's and B. Hoffmann's research teams [6, 7]. However, until recently, insufficient data on the macrocycles containing strong electron-withdrawing peripheral substituents such as CN groups formed a

Table 1. UV/Vis spectroscopy data for vanadyl complexes [5, 10]

Complex	**IIa**	**IIb**	**IIc**
UV/Vis spectrum: λ_{max}, nm (log ε)*	Soret band: 350 (4.65) Q-band: 610 (4.08), 672 (4.25)	Soret band: 345 (4.90) Q-band: 602 (4.27), 677 (4.29)	Soret band: 345 (4.98) Q-band: 620 (4.35), 720 (4.05)

* In tetrahydrofuran.

blank spot of the tetrapyrrole chemistry. This fact was noted with regret by Ghosh et al. [8], whose calculations have shown good prospects of using such macrocycles as catalysts for oxidation of organic compounds.

We have accomplished for the first time the template assembly of a macrocyclic octacyanoporphyrazine structure using tetracyanoethylene (TCNE) molecules as structural units [4]. It is noteworthy that the reaction proceeds under mild conditions (room temperature) and with high yields. The reaction of TCNE with bis(arene)vanadium ($V^0(arene)_2$) in an inert environment described previously [9], which we used for this purpose, gives a product insoluble in any solvent and behaving as a high-temperature molecular magnet. As noted by the authors, the ferromagnetism of the reaction products immediately disappears on contact with air or moisture; however, they do not present data on the chemical reasons behind the sharp changes in the magnetic properties of the obtained compounds. We found that this reaction has an unexpected continuation if the reaction mixture is brought in contact with oxygen or air moisture: the insoluble precipitate formed in the first stage ($V(TCNE)_x \cdot y$MeCN) gradually passes to the solution, which acquires a bright green color. The ESR spectrum of the acetonitrile solution showed an anisotropic signal for V=O with $g_{\|} = 1.960$, $g_{\perp} = 1.978$, and $a_{\perp} = 56$ G, which is typical of vanadyl porphyrazine complexes. The IR spectrum exhibits bands inherent in porphyrazines: macrocycle skeletal vibrations (1500 cm^{-1}), pyrrole ring vibrations (1645 cm^{-1} for ν(C=N) and 1580 cm^{-1} for ν(C=C)), and ν(V=O) vibrations (990 cm^{-1}). The formation of the porphyrazine macrocycle was also confirmed by the UV/Vis spectrum, which showed a strong Soret band (393 nm) and a Q band (678 nm). The molar extinction coefficient (ε) of the major spectral bands is rather high (logε = 4.3), which is also characteristic of tetrapyrrole dyes. Thus, using TCNE molecules as structural units, we accomplished the first template assembly of the porphyrazine macrocycle containing eight CN groups at the periphery [4]. The presumptive mechanism of formation of vanadyl octacyanoporphyrazine (**I**) is depicted in Scheme 1.

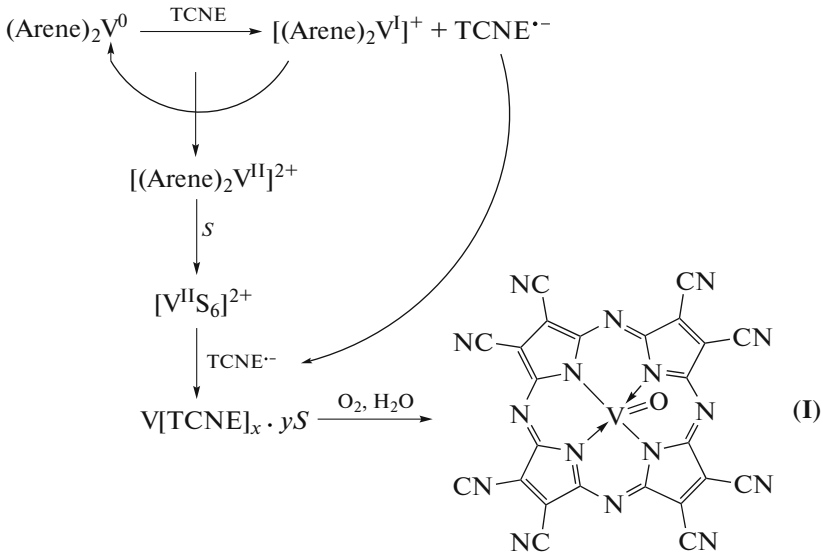

S = solvent

Scheme 1.

This facile approach proved to be quite useful for the synthesis of other cyano-containing porphyrazines. Using various aryltricyanoethylene molecules as structural units, we obtained new vanadyl tetra(aryl)tetracyanoporphyrazine complexes (Scheme 2) [5, 10].

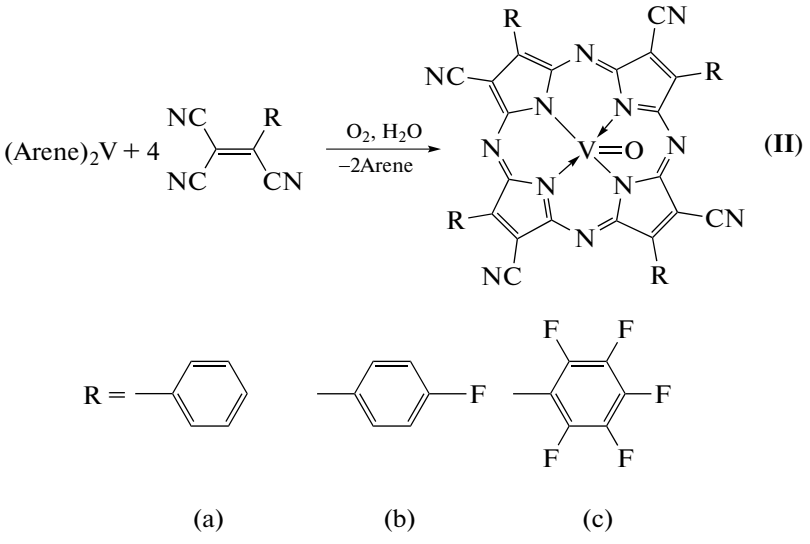

Scheme 2.

This provides the possibility of chemical design of the peripheral groups of porphyrazine macrocycles and fine tuning of their physicochemical properties (redox behavior and photophysical parameters) needed for various practical applications. The UV/Vis spectra of the presented metal complexes are also typical of porphyrazine dyes (Table 1). Interestingly, in the case of metal complex **IIc**, a considerable red shift of the Q band is observed.

The redox behavior of the vanadyl octacyanoporphyrazine complex has been studied by cyclic voltammetry in a DMF solution. The data presented in Table 2 indicate that vanadyl octacyanoporphyrazine is a strong acceptor capable of successive addition of, at least, four electrons. The first reduction potential (–0.08 V) is considerably higher than similar values for known porphyrazine macrocycles and their complexes. For example, the potential of vanadyl tetra-*tert*-butylporphyrazine is 0.7 V more negative [11]. There is only one known example of tetrapyrrole macrocycle (*tetrakis*(2,6-dichlorophenyl)heptanitroporphyrin) whose metal (zinc and nickel(II)) complexes are also strong electron acceptors [12]. Thus, the presence of eight peripheral cyano groups endows the vanadyl butyl(octacyano)porphyrazine complex with unique electron-withdrawing properties.

Using the correlation analysis proposed in [1, 13], we estimated the LUMO and HOMO energies from the first reduction and oxidation potentials, respectively. It should be noted that the oxidation potentials for vanadyl porphyrazine complexes were determined from the anodic peaks, because voltammograms attest to irreversibility of oxidation. However, it is known from published data that for cyclic voltammograms, the potentials determined in this way correspond to the half-wave potentials of reversible processes to within 0.01 V [13].

The LUMO energy for **I** is 3.9 eV (Table 2). Owing to the presence of a transition metal atom in the complex, an oxidative process also occurs rather easily in the system, evidently, via oxidation of vanadium(IV) in the vanadyl cation to vanadium(V). This accounts for the first oxidation potential being rather low (0.71 V) for such an efficient electron acceptor and the LUMO and HOMO energy difference, determining the band gap, being unusually small (1.1 eV) for an organic semiconductor. This value is much lower than the energy of the long-wavelength $\pi \rightarrow \pi^*$ transition (1.83 eV) observed in the spectrum of **I** (Q band). This

Table 2. Results of electrochemical investigations of vanadyl cyanoporphyrazine complexes [10]

Complex	Half-wave potentials $E_{1/2}$ vs. standard calomel electrode in DMF, V					Molecular orbital energies		
	reduction			oxidation		HOMO, eV	LUMO, eV	band gap, eV (nm)
I	–0.08	–0.70	–1.28	0.71	0.94	–5.0	–3.9	1.1 (1127)
IIa	–0.61	–1.51		0.80	1.38	–5.1	–3.1	2.0 (620)
IIb	–0.36	–0.80	–1.38					
IIc	–0.08	–0.39	–0.53	0.80		–5.1	–3.9	1.2 (1033)

means that the oxidation is metal-centered and is not directly related to electron transitions in the macrocycle, which is also confirmed by coincidence of the first oxidation potential of **I** with the potential of the V(IV)→V(V) redox pair in nitro-substituted Schiff bases [14].

A comparison of the electrochemical properties of complexes **IIa**, **IIb**, and **IIc** attests to considerable increase in the reduction potentials of metal complexes upon the introduction of fluorinated phenyl groups into the macrocycle periphery. This effect, which is especially pronounced for pentafluorophenyl peripheral substituents, makes compound **IIc** close in its reducing properties to vanadyl octacyanoporphyrazine complex [4]. Thus, we obtained a new tetrapyrrole dye, which possesses a rare combination of pronounced light absorption and electron-withdrawing properties unusually high for porphyrazine macrocycles. Furthermore, like the vanadyl octacyanoporphyrazine complex, compound **IIc** has a very narrow band gap (Table 2) [10]. For the vast majority of organic and polymeric semiconductors, this value exceeds 2 eV [15]. This means that the solar light absorption range for metal complex **IIc**, like for **I**, is considerably extended at the expense of the near-infrared region. This feature opens up the opportunity of using these compounds as new promising electron-acceptor components of compositions for fabrication of bulk heterojunction for organic photovoltaic devices [10].

The original synthetic approach described above, which provides the template assembly of cyanoporphyrazine macrocycles at room temperature with high yields, was modified by using the bis-indenyl ytterbium(II) π-complex $[(C_9H_7)_2Yb(THF)_2]$ as the initial sandwich metal complex (Scheme 3) [4, 5].

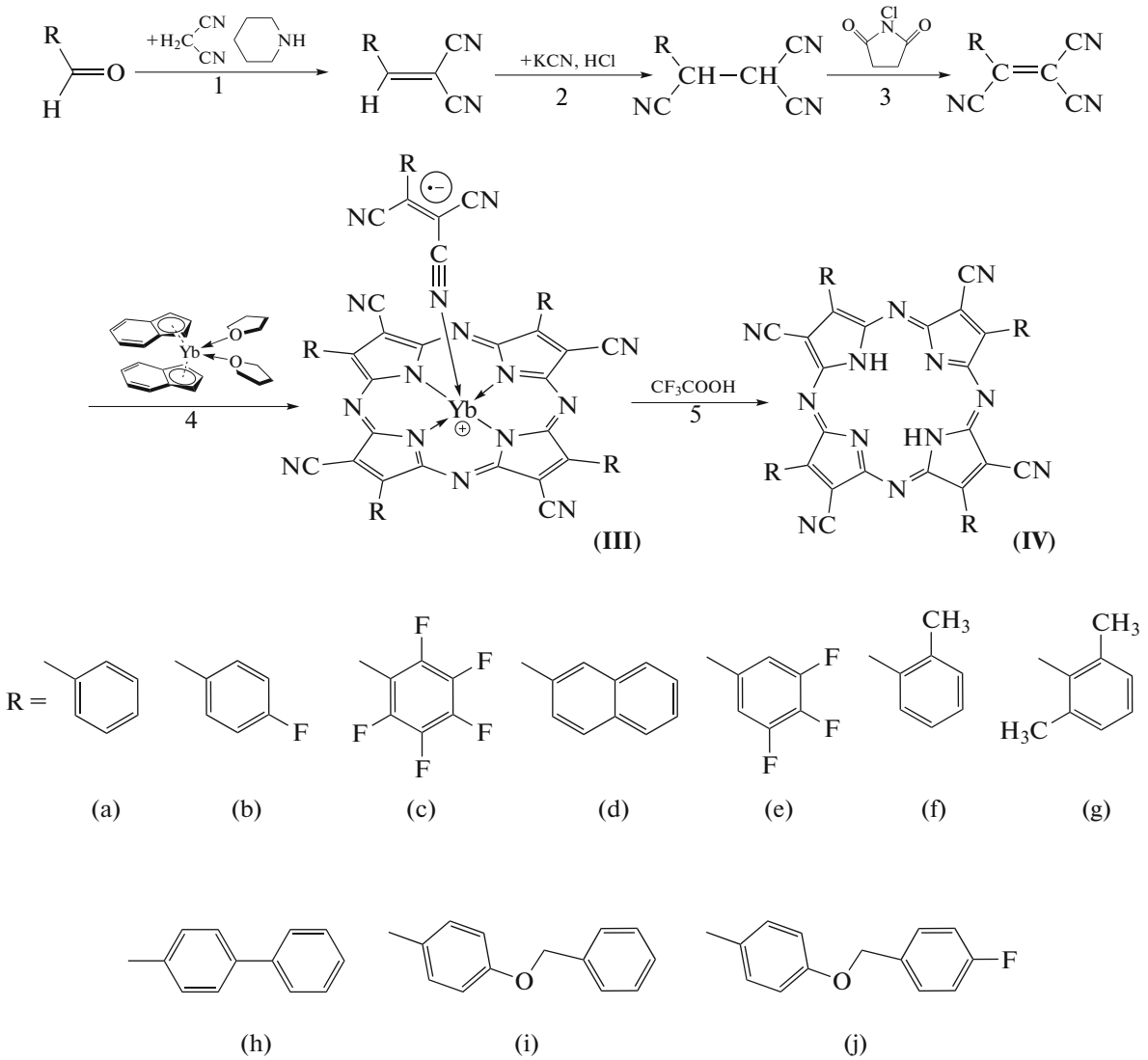

Scheme 3.

The template assembly of the macrocycle occurs on the Yb^{3+} cation. The porphyrazine metal complexes obtained in this way are more stable to air moisture. The scheme includes a three-stage preparation of the structural units for template assembly (aryltricyanoethylenes) from arenecarbaldehydes (Scheme 3, reactions 1–3) [16, 17]. An important distinction of the Yb^{3+}-assembled complexes from the vanadyl analogs is the possibility of demetallation with retention of the macrocyclic structure (Scheme 3; reactions 5 and 6), which may be attributable to their substantially higher hydrolytic stability. This gives a series of tetra(aryl)tetracyanoporphyrazines as free bases. It is noteworthy that variation of aromatic tricyanoethylene derivatives to be used for template synthesis of porphyrazine macrocycles is an efficient tool for the design of porphyrazine periphery, providing fine tuning of the chemical and photophysical properties of the dyes.

The UV/Vis spectra of all metal complexes and free bases exhibit Soret bands and Q bands typical of porphyrazines (Table 3) [17, 18]. All compounds possess high molar extinction coefficients, which is also typical of porphyrazine dyes. It is worth noting that the Q band absorption maximum is markedly shifted to longer wavelengths for free bases in comparison with the respective metal complexes. This is a benefit for a potential use in medicine, because it corresponds to the shift towards higher optical transparency of the biotissue.

TETRA(ARYL)TETRACYANOPORPHYRAZINES AS POTENTIAL PROBES FOR INTRACELLULAR VISCOSITY

An important structural feature of the tetra(aryl)tetracyanoporphyrazine dyes we obtained is alternation of electron-withdrawing (CN) and π-electron-donating aromatic groups located along the macrocycle frame and joined via the macrocycle conjugation system. The presence of electron-withdrawing and -donating groups involved in the common π-conjugation system in the dye molecule is known [19] to create conditions for intramolecular charge transfer from the donor to the acceptor upon excitation of the molecule with light. This, in turn, can lead to intramolecular motion of certain molecular groups (rotation or twisting), which has given rise to the name "molecular rotors" for this type of fluorescent dyes. The photophysical properties of these fluorophores are determined by the intramolecular rotation or twisting of certain molecular groups, resulting in dissipation of the excitation energy. Highly viscous media prevent this intramolecular motion, which results in an increase in the fluorescence intensity. Conversely, low viscosity of the medium is favorable for the motion of molecular groups and, hence, fluorescence considerably decays. This correlation can be described by the simple mathematical equations proposed by Förster and Hoffmann [20]:

$$\Phi_f = z\eta^{\alpha}, \quad (1)$$

$$\tau_f = zk_r^{-1}\eta^{\alpha}, \quad (2)$$

where Φ_f, τ_f, k_r, and η are the fluorescence quantum yield and lifetime, the rate constant for the excited to ground state radiative transition, and viscosity, respectively, and z and α are constants.

All of the tetraaryl(tetracyano)porphyrazine fluorophores we obtained exhibit a strong dependence of the fluorescence intensity on the viscosity of the medium [17, 18, 21]. For fluorescent molecular rotors, the slope of this dependence is known to be usually in the 1/3–2/3 range [22]. In the series of our porphyrazine macrocycles, the slope changes exactly in this range [17, 18, 21]. It is significant that in the case of porphyrazines with peripheral phenyl groups with *ortho*-substituted aromatic rings, the slope of the linear dependence of the quantum yield on the viscosity decreases. This attests to some decrease in the sensitivity of the fluorescence of these compounds to viscosity. Presumably, dissipation of the excitation energy of tetraaryl(tetracyano)porphyrazines in low-viscosity media occurs via the rotation of aryl substituents around the C–C bond, which is prevented by *ortho*-substituents in the aromatic ring.

It is noteworthy that the assignment of a fluorophore to the class of molecular rotors requires more stringent proof, including measurement of the dependence of the excited state lifetime (fluorescence lifetime) on the viscosity of the medium and the influence of the viscosity on the rate constants of radiative and non-radiative transitions in the molecule. The variation of the fluorescence lifetime of tetraaryl(tetracyano)porphyrazine macrocycles has been studied in detail for **IVb** [21]. The study was carried out in cooperation with UK researchers (Imperial College London, Chemical Department) by time-resolved laser spectroscopy. Quantitative relationships between fluorescence parameters and viscosity of the medium were found, suitable for the subsequent use for intracellular viscosity measurements. It was unambiguously proved that none of the parameters of the medium (solvent nature and dielectric permittivity, temperature fluctuations) affect the fluorescence properties of the macrocycles to such a great extent as viscosity. Figure 1 shows the fluorescence decay curves (λ_{emit} = 660 nm at λ_{excit} = 635 nm) in methanol–glycerol mixtures with known viscosity for the use of porphyrazine **IVb**. Table 4 gives the calculated fluorescence lifetimes **IVb** at various viscosity values. The fluorescence lifetime rapidly increases with increasing viscosity of the medium (Table 4, Fig. 1). A characteristic feature of the fluorescence of the given porphyrazines is the biexponential decay, which is indicative of the presence of two types of emission centers with dif-

Table 3. Data of UV/Vis spectroscopy for porphyrazines as ytterbium complexes and free bases

Porphyrazine	Absorption bands, nm*			Molar extinction coefficient, logε*	Porphyrazine	Absorption bands, nm*			Molar extinction coefficient, logε**
	Soret		Q			Soret		Q	
IIIa	330	399	598	4.29	**IVa**	328	398	616	4.42
IIIb	336	390	601	4.32	**IVb**	329	399	616	4.61
IIIc	325	416	618	4.24	**IVc**	325	413	632	4.46
IIId	329	392	615	4.48	**IVd**	330	409	620	4.55
IIIe	332	403	606	4.15	**IVg**	407	458	619, 590	4.32
IIIf	325	382	600	4.34	**IVf**	382	416	604	4.53
IIIh	356	401	613	4.19	**IVh**	350	410	615	4.25
IIIi	373	397	595, 640	4.35	**IVi**	360	397	616	4.40
IIIj	360	400	593	4.38	**IVj**	356	397	610	4.45

* In tetrahydrofuran. ** In water.

ferent fluorescence decay times (τ_1 and τ_2). It is of interest that the contribution (α) of "short-lived" emission centers to the fluorescence of porphyrazine **IVb** substantially decreases with increasing solution viscosity (increasing glycerol concentration) (Table 4). A fluorescent molecular rotor dissolved in a homogeneous medium can be characterized using the notion of average fluorescence lifetime (τ_{av}) determined from the formula

$$\tau_{av} = \frac{\Sigma a_i \tau_i^2}{\Sigma a_i \tau_i}. \quad (3)$$

The assumption that the obtained porphyrazine chromophores are molecular rotors is ultimately confirmed by the dependence of the rate constants of radiative (k_r) and non-radiative (k_{nr}) transitions on the viscosity. For porphyrazines **IVb** and **IVf**, the rate constants of radiative and non-radiative transitions were calculated from the fluorescence parameters (Φ_f and τ_{av}, equation (4)) [22].

$$\Phi_f = \frac{k_r}{k_r + k_{nr}} = k_r \tau_{av}. \quad (4)$$

Figure 2 shows the dependence of each rate constant on the viscosity. As the viscosity increases to 4000 cP, k_r remains virtually invariable for both porphyrazines, whereas k_{nr} sharply decreases. This means that at high viscosity of the medium, the non-radiative transitions are suppressed, which is typical of molecular rotors. Thus, the other obtained porphyrazines, analogues of **IVb** and **IVf**, can also be classified as molecular rotors, because the characteristic increase in the fluorescence quantum yield with increasing viscosity is also observed for these compounds (Fig. 2).

High viscosity sensitivity of fluorescence parameters of the dyes opens up the opportunity for using them as optical probes of viscosity. This information is of particular value for biological systems, because viscosity determines the rate of diffusion and, hence, the rate of bimolecular intracellular reactions, which affect the vital activity of the whole body. Pronounced changes in the intracellular viscosity lead to a severe change in the functional state of the cells and even to cell death. The efficiency of using fluorescent molecular rotors for determining the intratissue viscosity of a tumor has been recently shown for experimental animals (in vivo) [23]. The photoinduced cell death during photodynamic therapy was shown to be accompanied by a pronounced increase in the intracellular viscosity [24]. The optical probing of viscosity by fluorescent dyes behaving as molecular rotors can be used to monitor photodynamic therapy (PDT). This is especially convenient when the photosensitizer serves simultaneously as the probe of intracellular viscosity. Thus, the use of fluorescent molecular rotors as highly sensitive non-interventional optical probes of intracellular viscosity presents considerable interest for the design of new agents for diagnosis and therapy for personalized medicine.

DESIGN OF A LABORATORY MODEL OF A LUMINESCENT SOLAR CONCENTRATOR

It is known that the amount of electrical energy generated using photoelectric converter (PECs) can be increased by using solar light concentrators. Usually, these concentrators are large movable mirrors that follow the sun and focus the sunlight on the PECs. The manufacture and maintenance of such cumbersome movable devices are fairly expensive, which precludes a considerable decrease in the cost of energy production from solar light. Furthermore, the PECs located at the focus of a mirror concentrator are subjected to strong heating, which soon deteriorates their photo-

voltaic characteristics; therefore, a special cooling system is needed.

A pronounced optical concentration of solar light can also be achieved in fixed devices without superfluous heating of solar cells. This can be done using a luminescent solar concentrator (LSC), which is a waveguide made as an optically transparent glass or plastic sheet with incorporated luminescent organic dye. The dye efficiently absorbs light at a definite wavelength and emits it into the waveguide material, thus providing targeted delivery of the re-emitted energy to the solar cells attached at the concentrator end faces. The solar light concentration effect is caused by the many-fold difference between the light collection and re-emission areas [2].

We used a new approach to selection of components of a luminescent composition generating an additional flux of re-emitted solar light close to the absorption maximum wavelength of the porphyrazine dye (600–630 nm) upon excitation of the photoluminescence of luminophores incorporated in LSC in the near-UV range (340–390 nm) [25]. Compound **IIIb** was used as the main light-emitting component. The polycarbonate–dimethyl methacrylate/urethane dimethacrylate copolymer obtained by layer-by-layer photopolymerization served as the optical waveguide material.

We manufactured defect-free luminescent glasses from a polymer of this type doped with **IIIa** (Fig. 3). Excitation at 530–600 nm produces an efficient emission at 630 nm. The Stokes shift thus observed (not more than 30–35 nm) and the excited state lifetime (more than 3–6 ns) attest to the fluorescent mechanism of emission typical of dyes in which the radiative transition takes place from the excited singlet state (S_1) to the ground singlet state (S_0) of the macrocyclic ligand [5]. The photoluminescence quantum yield for this glass at 630 nm (λ_{excit} = 600 nm) is ~65%.

In order to make up for the self-absorption optical losses, which are inevitable due to overlap of the absorption and emission spectra, and to increase the luminescence quantum yield of the porphyrazine macrocycle, we added europium benzoyltrifluoromethylacetonate trihydrate $Eu(BTFA)_3 \cdot 3H_2O$, whose luminescence properties in organic glass matrix were studied previously [25]. This metal chelate is able to absorb solar energy in the near-UV range and exhibits

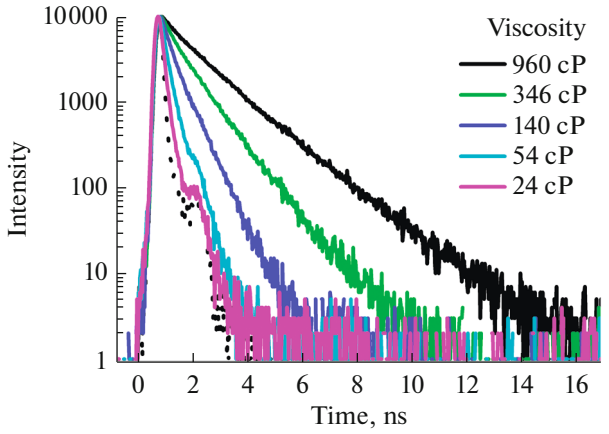

Fig. 1. Fluorescence decay curves for porphyrazine **IVb** (λ_{emit} = 660 nm at λ_{excit} = 635 nm) in methanol–glycerol mixtures with a known viscosity.

intense Eu^{3+} luminescence at 617 nm. The $Eu(BTFA)_3 \cdot 3H_2O$ to **IIIb** ratio was 10 : 1 (w/w). The europium and ytterbium complexes are capable of host–guest interactions in which the host molecules efficiently transfer the energy to the emission levels of the guest by the Förster mechanism, that is, as the inductive resonance energy between two chromophores (from the donor to the acceptor) without intermediate photon emission.

The data of Fig. 4 actually show a considerable increase in the emission of **IIIb** in the presence of the europium chelate. In addition, we found that the use of $Eu(BTFA)_3 \cdot 3H_2O$ as a host component gives additional benefits regarding the photon collection efficiency due to extending the light absorption range and additional re-emission. Our results gave grounds for using the developed material in the fabrication of a model LSC specimen based on photocurable low-defect organic glasses doped with complexes **IIIb** and $Eu(BTFA)_3 \cdot 3H_2O$ (Fig. 5) [25].

The key characteristics of LSCs is the efficiency of solar energy conversion by a photovoltaic cell with the use of a concentrator (η_{LSC}), geometric factor equal to the ratio between the surface areas of the illuminated part of the concentrator and PEC (G), and the energy concentration factor (F). The latter is calculated by the formula

Table 4. Calculated fluorescence lifetimes for **IVb**

MeOH	Glycerol	Viscosity, cP	τ_1, ns	α_1, %	τ_2, ns	α_2, %	τ_{av}, ns
0	100	960	0.49	18.01	1.62	81.99	1.55
10	90	346	0.31	25.18	0.99	74.82	0.93
20	80	140	0.17	31.34	0.55	68.66	0.50
30	70	54	0.07	37.81	0.27	62.19	0.24
40	60	24	0.03	59.98	0.15	40.02	0.12

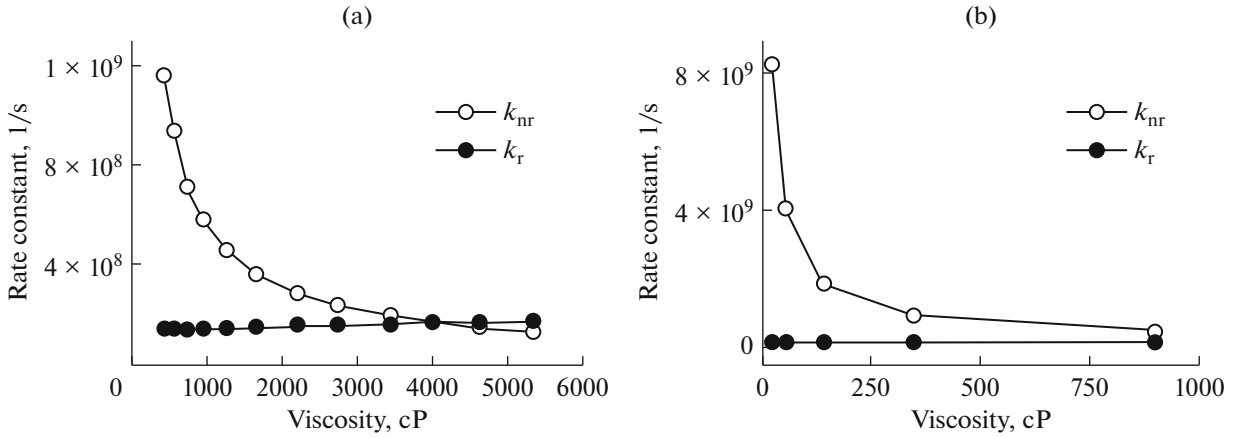

Fig. 2. Rate constants for radiative (k_r) and non-radiative (k_{nr}) transitions vs. viscosity of the methanol–glycerol mixture at 22°C for (a) **IVb** and (b) **IVf**.

$$F = \frac{G\eta_{LSC}}{\eta_{PEC}}, \quad (5)$$

where η_{PEC} is the photovoltaic cell efficiency. Table 5 presents characteristics of a model LSC specimen based on **IIIb**, measured in our study, and analogous data for LSCs based on luminophores—4-(dicyanomethylene)-2-*tert*-butyl-6-(1,1,7,7-tetramethyljulolidin-9-enyl)-4H-pyran (DCJTB) and platinum tetraphenyltetrabenzoporphyrin complex [Pt(TPBP)] [2]. The LSC we proposed was not inferior in the energy conversion efficiency to a similar device based on DCJTB, while the phosphorescent complex [Pt(TPBP)]) provided a markedly lower η_{LSC} value (Table 5). It is noteworthy that in our study, we used the most commercially available silicon PEC, whereas the authors of [2] performed measurements for specially selected photovoltaic cells whose spectral sensitivity ranges matched as close as possible the photoluminescence spectra of each chromophore. Nevertheless, the η_{LSC}/η_{PEC} ratio was much higher for the device that we fabricated than for single-level LSCs reported in [2], which is indicative of its higher efficiency. It is especially important that the LSC based on **IIIb** had a considerably higher energy concentration factor, which is an important characteristic of devices of this type. It is of interest that [Pt(TPBP)], which ensures almost zero self-absorption losses, is still much inferior in efficiency to **IIIb** as a luminophore. As noted by the authors of [2], a negative consequence of the phosphorescence effect, which ensures the greatest Stokes shift in the case of [Pt(TPBP)], is a decrease in the open-circuit voltage of the photovoltaic cell.

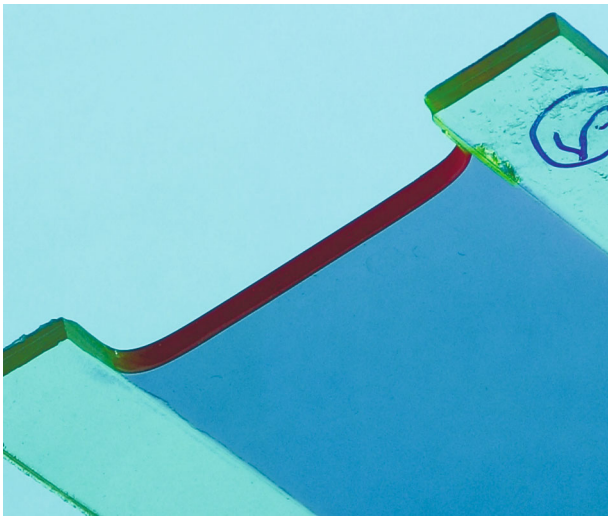

Fig. 3. Luminescent glass based on polycarbonate–dimethyl methacrylate doped with ytterbium tetraphenyltetracyanoporphyrazine complex **IIIa** (in 0.01 wt % concentration).

Thus, our results of testing the model LSC based on a new ytterbium cyanoporphyrazine complex **IIIb** and low-defect organic glass demonstrated the possibility of manufacturing fixed solar energy concentrators, which are not inferior in their characteristics to the best world prototypes of these devices.

BIOMEDICAL ASPECTS OF POSSIBLE PRACTICAL APPLICATION OF TETRA(ARYL)TETRACYANOPORPHYRAZINES

All the fluorescent porphyrazine macrocycles that we obtained can be easily accumulated in living cells. Furthermore, confocal imaging using tetraaryl(tetracyano)porphyrazines revealed a considerable enhancement of their fluorescence inside the cells as compared with that observed for them in cell culture solutions. This fact is in good agreement with the photophysical behavior of these dyes as fluorescent molecular rotors: evidently, dyes are localized inside

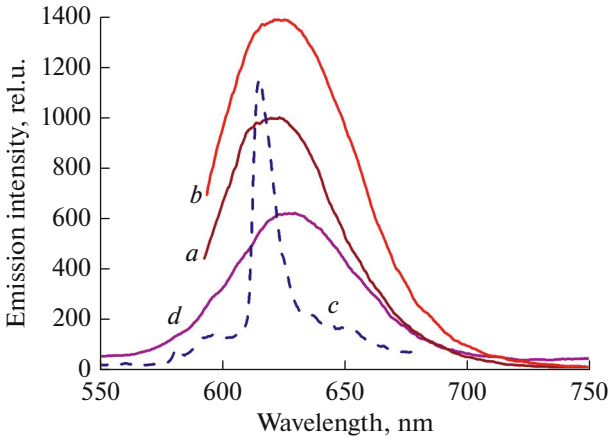

Fig. 4. Luminescence spectra of polycarbonate–dimethacrylate films containing (*a*) **IIIb** (0.05 wt %) at λ_{excit} = 580 nm and (*b–d*) **IIIb** (0.05 wt %) and $Eu(BTFA)_3 \cdot 3H_2O$ (0.5 wt %) at λ_{excit} = (*b*) 580, (*c*) 340, and (*d*) 390 nm. The film thickness is 200 μm.

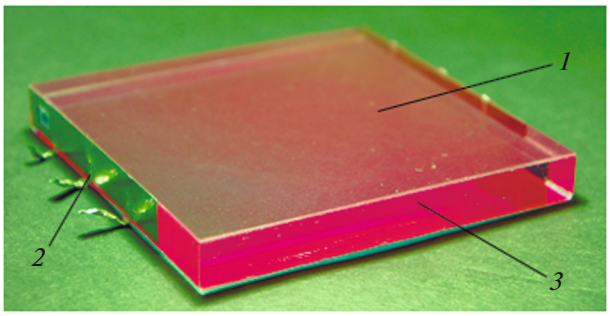

Fig. 5. Single-level LSC model: (*1*) luminescent surface layer doped with $Eu(BTFA)_3 \cdot 3H_2O$; (*2*) standard silicon solar cells manufactured by the LLC SOLTEK, Nizhny Novgorod, (*3*) optical waveguide based on low-defect organic glass (polycarbonate–dimethyl methacrylate/urethane dimethacrylate) manufactured by the research and production enterprise Reper-NN.

the cells in such a way that the mobility of their molecular groups is markedly limited (Fig. 6) [21].

The ability of porphyrazines to be accumulated in the cells, discovered in our studies, provided grounds for testing some of our dyes as agents for fluorescence lifetime imaging in vivo [26, 27]. Porphyrazine is well accumulated in the model tumor and allows fluorescence visualization of the tumor in the body of an experimental animal (Fig. 7). The images were obtained by superimposing the photograph and the fluorescence signal, which is shown in the pseudocolor map. The tumor area is indicated by arrows [26].

The fluorescence signal was monitored for 36 h after the introduction of nanoparticles and the time of maximum accumulation of porphyrazine in the tumor was estimated (3–5 h). It is worth noting that in normal tissues, a considerable portion of porphyrazine was excreted within 24 h after the injection, while in the tumor, the chromophore was retained for longer periods.

A distinctive feature of porphyrazine free bases containing peripheral substituents with strong electron-withdrawing properties is relatively high acidity of their amino groups. As a result, in polar solvents, these macrocycles exist mainly as free dianions, which facilitates their interaction with metal cations [28]. Recently, we obtained a bimodal agent for tumor diagnosis based on tetraaryl(tetracyano)porphyrazines, which is suitable for contrasting a malignant tumor not only by means of fluorescence lifetime, but also by magnetic resonance imaging. This was attained by introducing a paramagnetic gadolinium(III) cation into the macrocycle. This non-interventional dual tumor diagnosis markedly increases the reliability of the diagnostic procedure [29]. The synthesis of gadolinium tetraaryl(tetracyano)porphyrazine complexes is shown in Scheme 4.

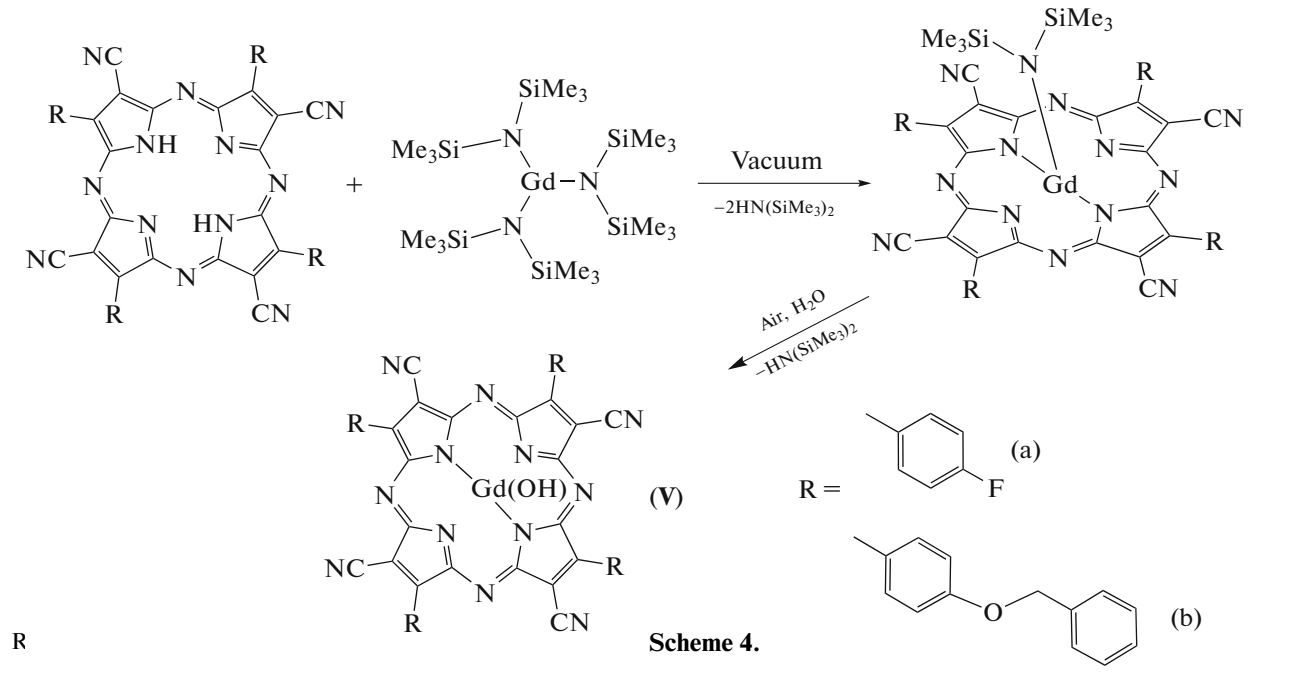

Scheme 4.

Table 5. Characteristics of LSCs based on low-defect glass made of a photocurable polymer composition, polycarbonate–dimethacrylate/urethane dimethacrylate containing **IIIb** [25] as a luminophore and LSCs reported in [2]

LSC	Luminophore	η_{LSC}, %	η_{PEC}, % (PEC type)	*G*	*F*
Single-level [25]	**IIIb**	5.4	10.5 (Si)	5.66	2.82
Multilevel [25]	$Eu(BTFA)_3 \cdot 3H_2O$/**IIIb**/Rhodamine 6G	11.3	13.8 (Si)		
Single-level [2]	[Pt(TPBP)]	4.1	25.1 (GaAs)	3.45	0.54
				5.66	0.88
Single-level [2]	DCJTB	5.9	18.1 (GaInP)	3.45	0.61
				5.66	1.13

As regards the possible therapeutic applications, an encouraging result was obtained in the studies of cytotoxic properties of the porphyrazines in the dark and on exposure to light. Tetraaryl(tetracyano)porphyrazines show a high photoinduced cytotoxicity, which gives hope for the development of efficient PDT sensitizers based on them [17, 30, 31]. It is well-known that PDT is widely used clinically for anticancer therapy.

Figure 8 shows the confocal microscopy data for the SK-OV-3 cells that have been subjected to the PDT procedure. Selective irradiation of an area of a cell culture induced dramatic changes in the morphological state of irradiated cells, indicative of their photoinduced death (compression, exfoliation, and bubble formation). The cell death was confirmed by characteristic change in their color, resulting from penetration of SYTOX® green, which is possible only upon serious damage of the protective cell membranes (Figs. 8a, 8b). The porphyrazine fluorescence spectra recorded before and after PDT do not differ from each other or from the fluorescence spectrum in glycerol. This means that porphyrazine itself, rather than the products of chain oxidation reactions initiated by reactive oxygen species, is the active agent responsible for the photoinduced death of SK-OV-3 cancer cells.

Using the SK-OV-3 cell line, we demonstrated the unique opportunities that can be opened in the future for dyes that combine the properties of photosensitizers and fluorescent molecular rotors. High sensitivity of fluorescence parameters to the medium viscosity allows real-time optical monitoring of the photodynamic therapy if there is a technical possibility to measure the fluorescence lifetime of the molecular rotor photosensitizer (Fig. 9) [21].

The selection of the optimal dose of laser irradiation of a tumor in each patient is still a challenge for the clinical application of PDT. This dose depends on the type and position of the laser irradiation source and the degree of tumor oxygenation. On cell cultures, we showed the possibility to detect changes in the fluorescence lifetimes for a photosensitizer possessing the molecular rotor behavior on a real time basis, which gives insight into the tumor dynamics during PDT, because changes of the fluorescence lifetime are correlated with the increase in the intracellular viscosity during the photoinduced cell death. The experiment was carried out by time-resolved fluorescence lifetime imaging microscopy (FLIM), which maps the cell image according to the lifetime of the photosensitizer loaded into it (Figs. 9a–9c).

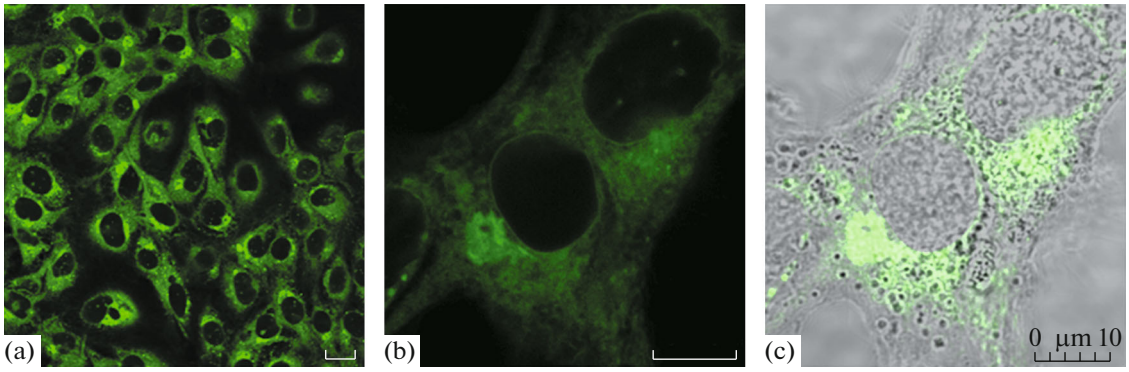

Fig. 6. (a, b) Confocal image of the SK-OV-3 cells after incubation with porphyrazine **IVb**. λ_{excit} = 561 nm, λ_{emit} = 600–800 nm. (c) Superimposed images of fluorescent and non-stained cells containing porphyrazine **IVb**. 2 μm scale in (a)and 1 μm scale in (b, c). [**IVb**] = 4 μM.

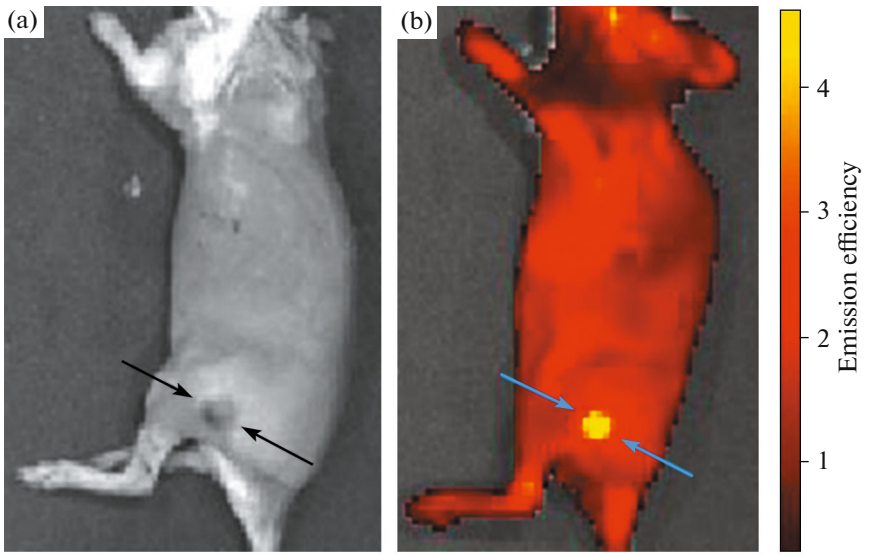

Fig. 7. Experimental animal (a) before and (b) 4 h after the administration of polymer brush-based nanoparticles doped with porphyrazine **IVb**.

Figure 9e shows the fluorescence lifetime of porphyrazine plotted vs. the cell irradiation time. The most pronounced increase in the photosensitizer fluorescence lifetime associated with the growth of viscosity occurs in the first 6 min. This can be considered to be the optimal irradiation time, because further treatment does not induce substantial changes in the functional state of cancer cells. The same is indicated by the fact that the amplitude of the fluorescence component with the longest lifetime stops to increase. The cell death was also confirmed by staining in the presence of SYTOX® green. Thus, the porphyrazine photosensitizer we developed can serve for determining the optimal dose and duration of light exposure for initiating the photodynamic therapy.

Our recent results about the effect of the 4-benzyloxy and 4-fluorobenzyloxy peripheral moieties of tetraaryl(tetracyano)porphyrazines on the cytotoxic properties are of interest for increasing the efficiency of porphyrazines as PDT sensitizers. The dark and photoinduced cytotoxicities (Table 6) of these compounds were evaluated against the A431 human epidermoid carcinoma cells. A widely used experimental method for this evaluation is to measure the inhibitory concentration IC_{50}, i.e., the content of the agent that induces a 50% decrease in the cell growth (or cell death). This value was measured both in the dark and under light irradiation. The resulting IC_{50} values are summarized in Table 6. Using Table 6, it is possible to compare the potential photodynamic activities of **IVi** and **IVj** with that of **IVb** described previously [21]. These results demonstrate that the three photosensitizers differ little in the inhibitory concentration characterizing the cell survival under irradiation (IC_{50}(light)). However, the inhibitory concentration measured in the dark (IC_{50}(dark)) is substantially higher for benzyloxy-substituted porphyrazines **IVi** and **IVj** than for **IVb**. This difference is especially impressive in the case of **IVj**, whose intrinsic cell toxicity (i.e., that not related to the photodynamic process) is more than an order of magnitude lower than that of **IVb** devoid of an oxygen atom in the peripheral substituents. This means that **IVi** and **IVj** are much more efficient PDT sensitizers than **IVb**, as the photocytotoxicity observed on irradiation is caused by photoinduced cell death to a much greater extent than by the undesirable intrinsic toxicity of the agent. The quantitative criterion of the photosensitizer quality is the IC_{50}(dark)/IC_{50}(light) ratio, corresponding to the so-called therapeutic index, which shows the range of safe use of a drug and represents the ratio of the toxic dose to the effective therapeutic dose. This value for **IVb** on cell cultures is very low, only 7.7, whereas that for **IVj** is 83. This gives hope for a high therapeutic index for this compound when used in vivo [18, 32]. Note that high dark cytotoxicity of PDT agents is a grave problem, causing severe undesirable side effects in patients. Therefore, we believe that the result we obtained could be useful in the future choice of approaches to the design of fluorescent tetrapyrrole structures with low dark cytotoxicity.

A problem related to the development of new diagnostic and therapeutic anticancer agents is solubilization in aqueous media and targeted delivery to the tumor. We developed two major approaches to the fabrication of biocompatible nano-sized polymeric forms of our porphyrazine photosensitizers. The first method is to encapsulate porphyrazine into macromolecular aggregates of biocompatible non-toxic water-soluble polymers reported in the literature (polyeth-

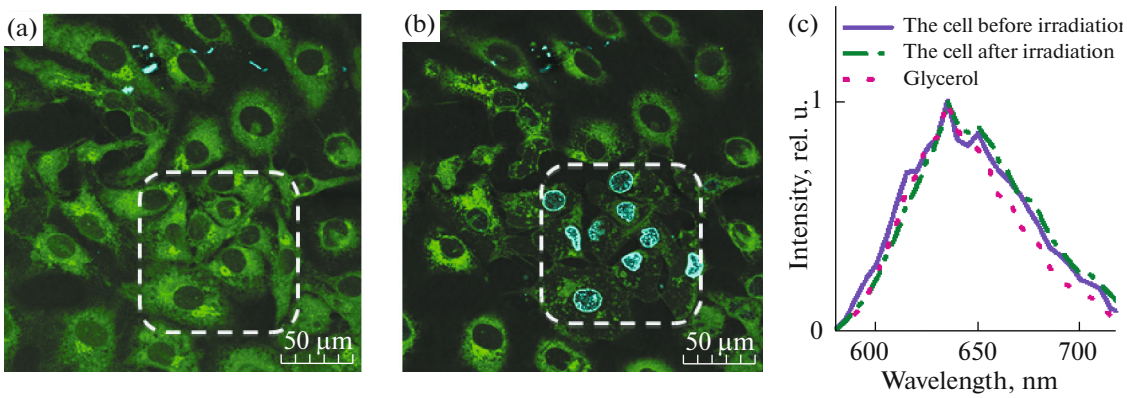

Fig. 8. (a, b) Are successively obtained fluorescent confocal images of the SK-OV-3 living cells containing porphyrazine **IVb** (4 μM) and SYTOX® green nucleic acid dye (1 μM) before and after 15-min irradiation of a sample area enclosed by dashed line. For porphyrazine, λ_{excit} = 561 nm and λ_{emit} = 650–759 nm; for SYTOX® green, λ_{excit} = 488 nm and λ_{emit} = 500–530 nm. (a) Before and (b) after 15-min irradiation of cells enclosed in a dashed-line square at λ_{excit} = 561 nm. 50 μm scale. (b) Are normalized fluorescence spectra of porphyrazine before and after irradiation and in glycerol at λ_{excit} = 561 nm, λ_{emit} = 590–785 nm [21].

ylene glycol (PEG), methylcellulose (MC), sodium alginate (AlgNa)) or a water-soluble polymer brush (PB) (graft copolymer obtained by acid hydrolysis of polyimide-graft-poly-*tert*-butyl methacrylate) developed at the Institute of Macromolecular Compounds under supervision of A.V. Yakimanskii [33]. The best result was obtained for the water-soluble PB. The addition of the PB in a minute quantity (not more than 0.07 wt %), which cannot noticeably affect the viscosity of an aqueous solution, provides not only efficient dissolution of the fluorophore in water, but also a considerable increase in the quantum yield. Moreover, we have found that the PB only delivers the photosensitizer to a cancer cell, but does not itself penetrate the cell.

The hydrodynamic diameters of various polymeric nanoparticles containing porphyrazine (**IVb**–polymer) were estimated and found to increase in the series **IVb**–PB < **IVb**–PEG < **IVb**–MC (Fig. 10). In the case of **IVb**–PB, the nanoparticle size was 114 ± 9 nm, which is optimal, considering the possible enhanced permeability and retention (EPR) effect of nanoparticles, related to the enhanced permeability of the "loose" blood circulatory system of a malignant tumor for nanoparticles of a definite size. The data of Fig. 11 indicate that "nanocontainers" based on other water-soluble polymers are markedly larger and the size scatter is greater: 474 ± 21 nm (**IVb**–PEG), 774 ± 93 nm (**IVb**–MC) [30].

Aqueous micellar solutions of tetraaryl(tetracyano)porphyrazines have high molar extinction coefficients at the long-wavelength maximum (ε ≈ 1.8 × 10^4 L mol^{-1} cm^{-1}), which is typical of most tetrapyrrole-based photosensitizers. Figure 12 shows the absorption and fluorescence spectra of **IVb**–polymer nanoparticles. The position of the absorption maximum does not depend on the nature of the polymer, and the height of the absorption peak changes insignificantly. The fluorescence intensity of **IVb**–polymer systems depends considerably on the nature of the polymer used (Fig. 12) and increases in the series **IVb**–PEG < **IVb**–MC < **IVb**–PB.

The fluorescence quantum yield of **IVb**–polymer nanoparticles in an aqueous solution is very low, about 5 × 10^{-3} to 7 × 10^{-3}, depending on the type of polymer. However, the red luminescence signal of porphyrazine chromophores was found to be enhanced by a large factor in the media containing blood proteins. An even more pronounced effect was observed in a 10% solution of serum albumin. In this case, the quantum yield was 0.7–0.8, which is two orders of magnitude higher than the value in water.

Table 6. IC_{50}* values for photoinduced and dark cytotoxicity of porphyrazines **IVb**, **IVi**, **IVj**

Porphyrazine	Photoinduced cytoyoxicity, IC_{50}(light), mol/L	Dark cytotoxicity, IC_{50}(dark), mol/L	IC_{50}(dark)/IC_{50}(light)
IVb	8.2 × 10^{-7}	6.3 × 10^{-6}	7.7
IVi	1.0 × 10^{-6}	4.0 × 10^{-5}	40.0
IVj	8.9 × 10^{-7}	7.4 × 10^{-5}	83.1

* IC_{50} is the concentration of the agent inducing a 50% decrease in the cell growth (or cell death).

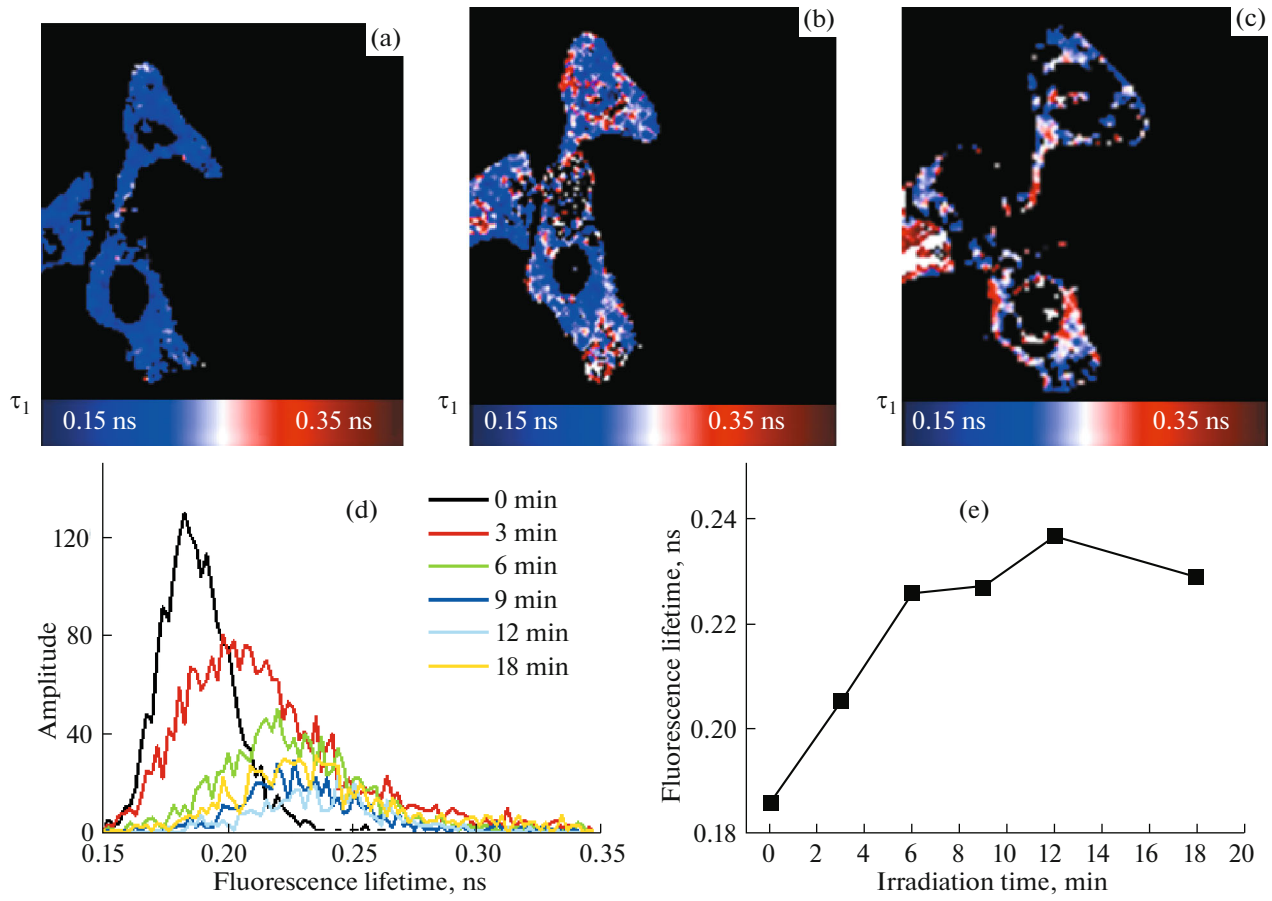

Fig. 9. (a, b) Are FLIM images of the SK-OV-3 cells with **IVa** (λ_{excit} = 561 nm, λ_{emit} = 600–750 nm): (a) before, (b) 3 min after, and (c) 18 min after irradiation. (d) Is the FLIM histogram of τ_1 obtained after different irradiation times, (e) is the dependence of τ_1 on the irradiation time.

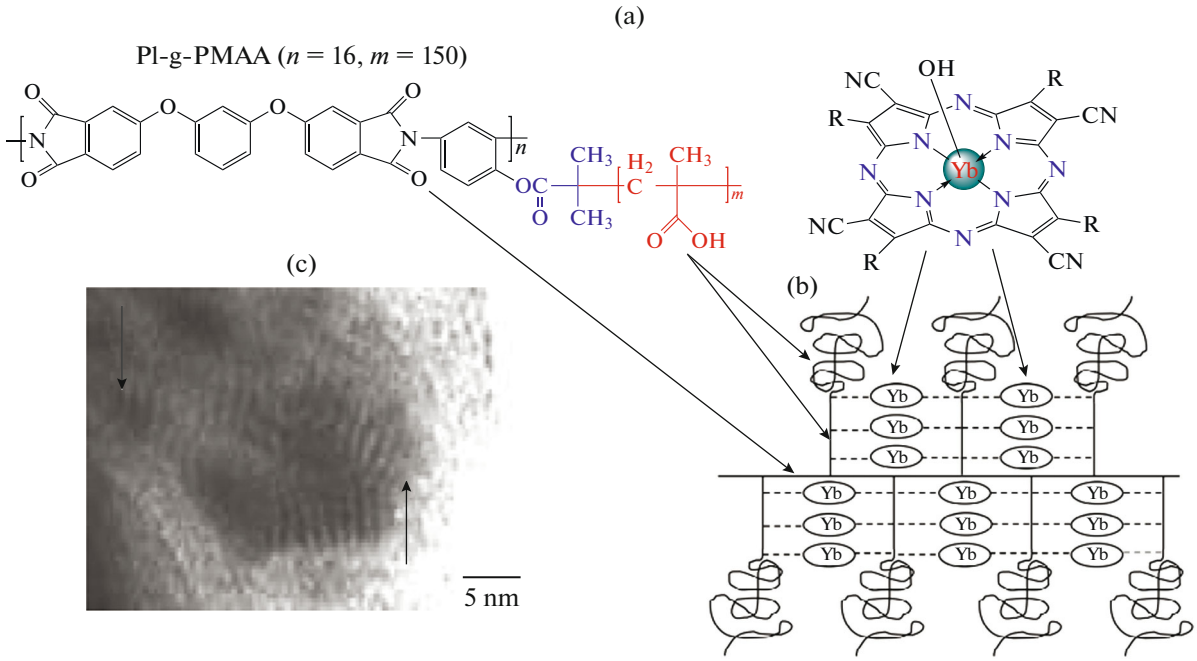

Fig. 10. Architecture of the polymer brush nanoconjugate of the porphyrazine macrocycle: (a) polymer brush structure; (b) assumed structure of the nanoconjugate; (c) TEM image of the nanoconjugate.

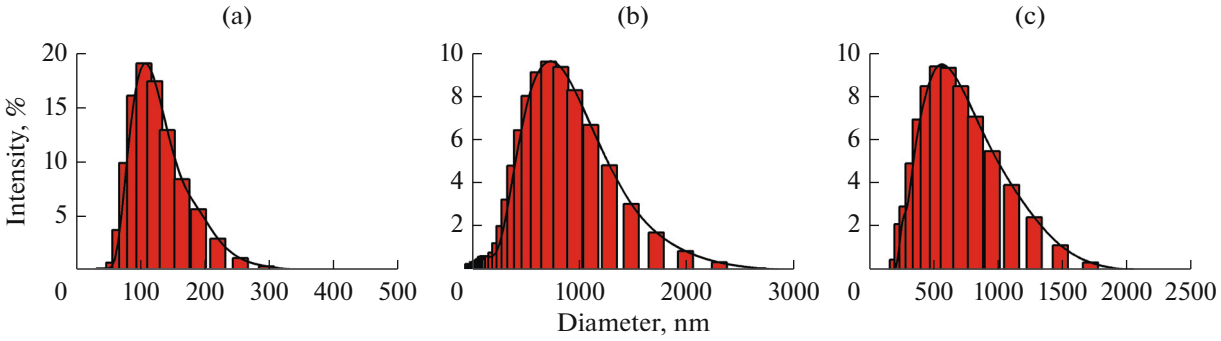

Fig. 11. Size distribution histogram of **IVb**–polymer nanoparticles: (a) **IVb**–PB; (b) **IVb**–MC; (c) **IVb**–PEG.

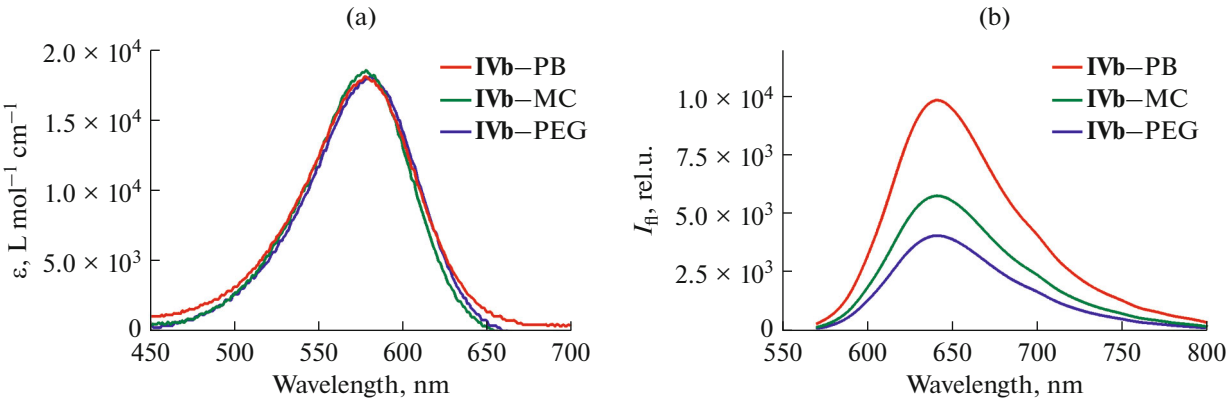

Fig. 12. (a) Absorption and (b) fluorescence spectra of **IVb**–polymer nanoparticles. The concentration of **IVb** is 5 μM; λ_{excit} = 560 nm.

A study of intracellular internalization and cell distribution of porphyrazine chromophores encapsulated into polymeric nanoparticles of various natures has shown that the type of polymer has a considerable effect on the fluorescence signal intensity; with the dye concentration being the same, the fluorescence intensity of **IVb** in the cell increased in the following series of polymers: PEG < MC ≅ AlgNa < PB (Fig. 12). In the absence of a solubilizing agent, the signal is comparable to that observed with the polymer brush. In the study of intracellular localization and cytotoxicity, the porphyrazine was introduced in the medium as a part of PB-based nanoparticles [30]. Their dark and photoinduced cytotoxicities were quantitatively estimated against the A431 human epidermoid carcinoma cells. The phototoxicity of **IVb**–PB was found to be markedly higher than the dark toxicity. The inhibitory concentration IC_{50} for this conjugate was 20 μM on irradiation in a 10 J/cm^2 dose and >60 μM in the dark.

It is worth noting that the polymer brush showed rather low cytotoxicity, which confirms good prospects for using PB for the delivery of a potential drug. Thus, we have found the following: among the tested polymers, polymer brush nanoparticles have the best prospects for the delivery of a photosensitizer to the tumor [29, 30].

ACKNOWLEDGMENTS

This work was supported by the RF Ministry of Education and Science (contract 14.Z50.31.0022).

REFERENCES

1. Borec, C., Hanson, K., Djirovich, P.I., et al., *Angew. Chem., Int. Ed. Engl.*, 2007, vol. 46, p. 1109.
2. Currie, M.J., Mapel, J.K., Heidel, T.D., et al., *Science*, 2008, vol. 321, p. 226.
3. Gel'fond, M.L., *Prakticheskaya Onkologiya*, 2007, vol. 8, p. 204.
4. Klapshina, L.G., Grigoryev, I.S., Douglas, W.E., et al., *Chem. Commun.*, 2007, no. 19, p. 1942.
5. Klapshina, L.G., Douglas, W.E., Grigoryev, I.S., et al., *J. Mater. Chem.*, 2009, vol. 19, p. 3668.
6. Michel, S.L.J., Hoffman, B.M., Baum, S.M., and Barrett, A.G.M., Carlin, K.D., Ed., New York: Wiley, 2001, p. 473.
7. Trivedi, E.R., Harney, A.S., Olive, M.E., et al., *PNAS*, 2010, vol. 107, p. 2084.

8. Ghosh, A., Gassman, P.G., and Almlöf, J., *J. Am. Chem. Soc.*, 1994, vol. 116, p. 1932.
9. Manriquez, J.M., Yee, G.T., McLean, R.S., et al., *Science*, 1991, vol. 252, p. 1415.
10. Grigor'ev, I.S., Lermontova, S.A., Klapshina, L.G., et al., *Dokl. Ross. Akad. Nauk.*, 2012, vol. 447, no. 4, p. 410.
11. Kobayashi, N., Nakajima, S., and Osa, T., *Chem. Lett.*, 1992, vol. 21, p. 2415.
12. Ozette, K., Leduc, P., Palacio, M., et al., *J. Am. Chem. Soc.*, 1997, vol. 119, p. 6442.
13. D'Andrade, B.W., Datta, S., Forrest, S.R., et al., *Organic Electronics*, 2005, vol. 6, p. 11.
14. Kianfar, A.H. and Mohebbi, S., *J. Iran. Chem. Soc.*, 2007, vol. 4, p. 215.
15. Günes, S.H., Neugebauer, H., and Sariciftci, N.S., *Chem. Rev.*, 2007, vol. 107, p. 1324.
16. Harvey, M.D., Pace, J.T., and Yee, G.T., *Polyhedron*, 2007, vol. 26, p. 2037.
17. Lermontova, C.A., Grigor'ev, I.S., Shilyagina, M.Yu., et al., *Russ. J. Gen. Chem.*, 2016, vol. 86, no. 6, p. 1330.
18. Lermontova, S.A., Grigor'ev, I.S., Peskova, N.N., et al., *Russ. J. Gen. Chem.*, 2017, vol. 87, no. 3, p. 479.
19. Haidekker, M.A. and Theodorakis, E.A., *J. Biol. Eng.*, 2010, vol. 4, p. 1.
20. Forster, V. and Hoffmann, G., *J. Phys. Chem.*, 1971, vol. 75, p. 63.
21. Izquierdo, M.A., Vysniauskas, A., Lermontova, S.A., et al., *J. Mater. Chem.*, vol. 3, no. 2015, p. 1089.
22. Kuimova, M.K., *Chimia*, 2012, vol. 66, p. 159.
23. Shimolina, L.E., Izquierdo, M.A., López-Duarte, I., et al., *Sci. Rep.*, 2017, vol. 7, article number: 41097.
24. Kuimova, M.K., Botchway, S.W., Parker, A.W., et al., *Nature Chemistry*, 2009, vol. 1, p. 69.
25. Grigor'ev, I.S., Klapshina, L.G., Lermonotova, S.A., et al., *Rossiiskie Nanotekhnologii*, 2012, vol. 7, nos. 9–10, p. 53.
26. Klapshina, L.G., Douglas, W.E., Grigoryev, I.S., et al., *Chem. Commun.*, 2010, vol. 46, p. 8398.
27. Klapshina, L.G., Kuimova, M.K., Balalaeva, I.V., et al., *Proceedings of IV International Symposium "Topical Problems of Biophotonics—2013*," Nizhny Novgorod, 2013, p. 160.
28. Kopranenkov, V.N. and Luk'yanets, E.A., *Izv. Akad. Nauk, Ser. Khim.*, 1995, no. 12, p. 2320.
29. Yuzhakova, D.V., Lermontova, S.A., Grigoryev, I.S., et al., *BBA General Subjects*, 2017, vol. 1861, p. 3120.
30. Shilyagina, N.Y., Peskova, N.N., Lermontova, S.A., et al., *J. Biophotonics*, 2017, vol. 10, p. 1189.
31. Klapshina, L.G., Lermontova, S.A., Grigoryev, I.S., et al., *Proceedings of VI International Symposium "Topical Problems of Biophotonics—2017."* St.-Petersburg–Nizhny Novgorod, 2017, p. 88.
32. Klapshina, L.G., Lermontova, S.A., Peskova, N.N., et al., RF Patent 2621710.
33. Yakimansky, A.V., Meleshko, T.K., Ilgach, D.M., et al., *J. Polym. Sci., Part A*, 2013, vol. 51, p. 4267.

Translated by Z. Svitanko